

Chapter 15

Novel Aspects of the Fabry-Pérot Resonator



Markus Pollnau and Nur Ismail

Abstract We systematically characterize the Fabry-Pérot resonator. We derive the generic Airy distribution of a Fabry-Pérot resonator, which equals the internal resonance enhancement factor, and show that all related Airy distributions are obtained by simple scaling factors. We verify that the sum of the mode profiles of all longitudinal modes generates the Airy distribution. Consequently, the resonator losses are quantified by the linewidths of the underlying Lorentzian lines and not by the measured Airy linewidth. We introduce the Lorentzian finesse which provides the spectral resolution of the Lorentzian lines, whereas the usually considered Airy finesse quantifies the performance of the Fabry-Pérot resonator as a scanning spectrometer.

15.1 Introduction

The Fabry-Pérot resonator which was invented in 1899 [1] has proven very useful as a high-finesse interferometer in uncountable spectroscopic applications. Since 1960, it has also formed the fundamental basis for a large class of open resonators that have enabled laser oscillation. The Fabry-Pérot resonator has been extensively investigated, experimentally as well as theoretically. However, when the losses become high, discrepancies between the theoretical approaches surface, common approximations turn invalid, and even the definitions of typical parameters break down or prove inappropriate.

M. Pollnau (✉)

Department of Electrical and Electronic Engineering, Advanced Technology Institute, University of Surrey, Guildford, UK

Department of Materials and Nano Physics, KTH—Royal Institute of Technology, Electrum 229, Kista, Sweden

e-mail: m.pollnau@surrey.ac.uk

N. Ismail

Department of Materials and Nano Physics, KTH—Royal Institute of Technology, Electrum 229, Kista, Sweden

We analyze the performance and relevant parameters of the Fabry-Pérot resonator, with reference to the book on the Fabry-Pérot resonator by Vaughan [2] and the standard text books by Siegman [3], Svelto [4, 5], and Saleh and Teich [6–8]. We demonstrate that the sum of the mode profiles of all longitudinal modes, which are Lorentzian-shaped in case of frequency-independent losses, is the fundamental spectral function that characterizes the Fabry-Pérot resonator. It physically generates the Airy distribution of the Fabry-Pérot resonator. The resonator losses are quantified by the linewidths of the underlying Lorentzian lines. We define the Lorentzian finesse which provides the resolution of the Lorentzian lines, whereas the usually considered Airy finesse describes the performance of the Fabry-Pérot resonator as a scanning spectrometer.

15.2 Resonator Losses and Outcoupled Light

Throughout this paper, we assume a two-mirror Fabry-Pérot resonator of geometrical length ℓ , homogeneously filled with a medium of refractive index n_r . Both, ℓ and n_r are assumed to vary insignificantly over the frequency range of interest. The round-trip time t_{RT} of light travelling in the resonator with speed $c = c_0/n_r$, where c_0 is the speed of light in vacuum, is given by

$$t_{RT} = \frac{2\ell}{c}. \quad (15.1)$$

Outcoupling losses occur due to non-perfect reflectivity of the two mirrors,

$$r_i^2 = R_i = 1 - t_{out,i}^2 = 1 - T_{out,i} = e^{-t_{RT}/\tau_{out,i}} \iff \frac{1}{\tau_{out,i}} = \frac{-\ln(R_i)}{t_{RT}} = \frac{-\ln(1-T_{out,i})}{t_{RT}}. \quad (15.2)$$

Here, $r_i(\nu)$ and $R_i(\nu)$ are the electric-field and intensity reflectivities, respectively, $t_{out,i}(\nu)$ and $T_{out,i}(\nu)$ are the electric-field and intensity transmissions, respectively, and $\tau_{out,i}(\nu)$ is the exponential decay time resulting from the outcoupling loss at mirror i . All other losses shall be neglected. The photon-decay time $\tau_c(\nu)$ of the resonator is then given by

$$\frac{1}{\tau_c} = \sum_i \frac{1}{\tau_{out,i}} = \frac{\sum_i \delta_{out,i}}{t_{RT}} = \frac{\sum_i -\ln(R_i)}{t_{RT}}. \quad (15.3)$$

The number $\varphi(t)$ of photons at frequency ν , present inside the resonator at time t , is described via the photon-decay time $\tau_c(\nu)$ by the differential rate equation

$$\frac{d}{dt}\varphi(t) = -R_{decay}(t) = -\frac{1}{\tau_c}\varphi(t). \quad (15.4)$$

$R_{decay}(t)$ is the photon-decay rate per unit time. With a number φ_s of photons present at the starting time $t = 0$, integration delivers

$$\varphi(t) = \varphi_s e^{-t/\tau_c}. \quad (15.5)$$

With $\phi(\nu)$ quantifying the single-pass phase shift between the mirrors, the round-trip phase shift at frequency ν accumulates to

$$2\phi(\nu) = 2\pi\nu t_{RT} = 2\pi\nu \frac{2\ell}{c}. \quad (15.6)$$

We have assumed above that the refractive index n_r of the medium and, thus, the speed of light c are independent of frequency. Consequently, also the round-trip time t_{RT} becomes independent of frequency. Resonances occur at frequencies at which light exhibits constructive interference after one round trip. The difference in phase shift per round trip between adjacent resonance frequencies amounts to 2π , from which the free spectral range $\Delta\nu_{FSR}$ then derives as [2].

$$\frac{d}{d\nu}(2\phi) = \frac{d}{d\nu}(2\pi\nu t_{RT}) = 2\pi t_{RT} \Rightarrow \frac{2\pi}{\Delta\nu_{FSR}} = 2\pi t_{RT} \Rightarrow \Delta\nu_{FSR} = \frac{1}{t_{RT}}. \quad (15.7)$$

Each resonator mode with its mode index q , where q is an integer number in the interval $[-\infty, \dots, -1, 0, 1, \dots, \infty]$, is associated with a resonance frequency ν_q and wavenumber k_q ,

$$\nu_q = q\Delta\nu_{FSR} = q/t_{RT} \Rightarrow k_q = \frac{2\pi q\Delta\nu_{FSR}}{c}. \quad (15.8)$$

Two modes with opposite values $\pm q$ and $\pm k$ of modal index and wavenumber, respectively, physically representing opposite propagation directions, occur at the same absolute value $|\nu_q|$ of frequency.

According to Eq. (15.5), light at frequency ν oscillating inside the resonator decays out of the resonator with a time constant of $\tau_c(\nu)$. If the resonator losses are independent of frequency, the photon-decay time $\tau_c(\nu)$ is the same at all frequencies. The decaying electric field at frequency ν_q is represented by a damped harmonic oscillation with an initial amplitude of $E_{q,s}$ and a decay-time constant of $2\tau_c$. In phasor notation, it can be expressed as

$$E_q(t) = \begin{cases} E_{q,s} e^{i2\pi\nu_q t} e^{-t/(2\tau_c)} & t \geq 0 \\ 0 & t < 0 \end{cases}. \quad (15.9)$$

Fourier transformation of the electric field in time provides the electric field per unit frequency interval,

$$\begin{aligned}\tilde{E}_q(\nu) &= \int_{-\infty}^{+\infty} E_q(t) e^{-i2\pi\nu t} dt = E_{q,s} \int_0^{+\infty} e^{-[1/(2\tau_c) + i2\pi(\nu - \nu_q)]t} dt \\ &= E_{q,s} \frac{1}{(2\tau_c)^{-1} + i2\pi(\nu - \nu_q)}.\end{aligned}\quad (15.10)$$

Each mode has a normalized spectral line shape per unit frequency interval given by [9].

$$\begin{aligned}\tilde{\gamma}_q(\nu) &= \frac{1}{\tau_c} \left| \frac{\tilde{E}_q(\nu)}{E_{q,s}} \right|^2 \\ &= \frac{1}{\tau_c} \left| \frac{1}{(2\tau_c)^{-1} + i2\pi(\nu - \nu_q)} \right|^2 = \frac{1}{\tau_c} \frac{1}{(2\tau_c)^{-2} + 4\pi^2(\nu - \nu_q)^2} \\ &= \frac{1}{\pi} \frac{1/(4\pi\tau_c)}{1/(4\pi\tau_c)^2 + (\nu - \nu_q)^2} \quad \text{with} \quad \int \tilde{\gamma}_q(\nu) d\nu = 1,\end{aligned}\quad (15.11)$$

in units of (1/Hz). Introducing the full-width-at-half-maximum (FWHM) linewidth $\Delta\nu_c$ of the Lorentzian spectral line shape, we obtain

$$\Delta\nu_c = \frac{1}{2\pi\tau_c} \Rightarrow \tilde{\gamma}_q(\nu) = \frac{1}{\pi} \frac{\Delta\nu_c/2}{(\Delta\nu_c/2)^2 + (\nu - \nu_q)^2} \quad \text{with} \quad \int \tilde{\gamma}_q(\nu) d\nu = 1.\quad (15.12)$$

Calibrated to a peak height of unity, we obtain the Lorentzian lines, in units of (1):

$$\gamma_{q,L}(\nu) = \frac{\pi}{2} \Delta\nu_c \tilde{\gamma}_q(\nu) = \frac{(\Delta\nu_c)^2}{(\Delta\nu_c)^2 + 4(\nu - \nu_q)^2} \quad \text{with} \quad \gamma_{q,L}(\nu_q) = 1.\quad (15.13)$$

When repeating the above Fourier transformation for all the modes with mode index q in the resonator, one obtains the full mode spectrum of the resonator.

15.3 Airy Distributions of the Fabry–Pérot Resonator

In this Section, we derive the generic Airy distribution, show that it represents the spectral dependence of the internal resonant enhancement factor, and demonstrate that all other Airy distributions describing the circulating, back-circulating, transmitted, and back-transmitted intensity (Fig. 15.1) only include simple scaling factors, depending on whether the light incident upon mirror 1 or its fraction

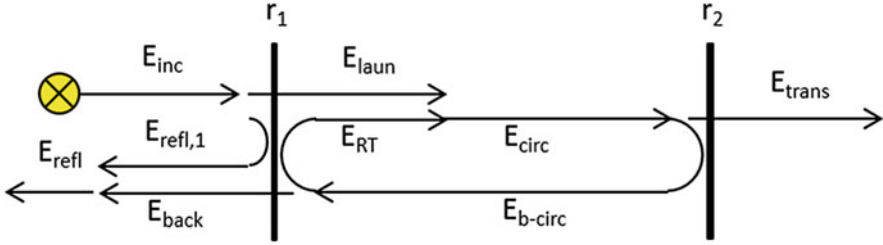


Fig. 15.1 Fabry-Pérot resonator with electric-field mirror reflectivities r_1 and r_2 . Indicated are the characteristic electric fields produced by an electric field E_{inc} incident upon mirror 1: $E_{refl,1}$ initially reflected at mirror 1, E_{laun} launched through mirror 1, E_{circ} and E_{b-circ} circulating inside the resonator in forward and backward propagation direction, respectively, E_{RT} propagating inside the resonator after one round trip, E_{trans} transmitted through mirror 2, E_{back} transmitted through mirror 1, and the total field E_{refl} propagating backward. Interference occurs at the left- and right-hand sides of mirror 1 between $E_{refl,1}$ and E_{back} , resulting in E_{refl} , and between E_{laun} and E_{RT} , resulting in E_{circ} , respectively. (Figure taken from Ref. [10])

launched into the resonator is considered as a reference. We verify that the physical origin of the Airy distribution is the sum of mode profiles of the longitudinal resonator modes.

15.3.1 Generic Airy Distribution: The Internal Resonance Enhancement Factor

The response of the Fabry-Pérot resonator is most easily derived by use of the circulating-field approach [3], as displayed in Fig. 15.1. This approach assumes a steady state and derives the Airy distributions via the electric field E_{circ} circulating inside the resonator. In fact, E_{circ} is the field propagating in the forward direction from mirror 1 to mirror 2 after interference between the field E_{RT} that is circulating after one round trip, i.e., after having suffered outcoupling losses at both mirrors, and the field E_{laun} launched through the first mirror.

With the phase shift 2ϕ of Eq. (15.6) accumulated in one round trip, the field E_{circ} can be related to the field E_{laun} that is launched into the resonator in the situation of Fig. 15.1a by

$$E_{circ} = E_{laun} + E_{RT} = E_{laun} + r_1 r_2 e^{-i2\phi} E_{circ} \Rightarrow \frac{E_{circ}}{E_{laun}} = \frac{1}{1 - r_1 r_2 e^{-i2\phi}}. \quad (15.14)$$

Exploiting the identities

$$\begin{aligned} |e^{-i\phi}|^2 &= |\cos(\phi) - i \sin(\phi)|^2 = \cos^2(\phi) + \sin^2(\phi) = 1 \\ \cos(2\phi) &= 1 - 2\sin^2(\phi) \end{aligned} \quad (15.15)$$

yields

$$\begin{aligned}
 |1 - r_1 r_2 e^{-i2\phi}|^2 &= |1 - r_1 r_2 \cos(2\phi) + i r_1 r_2 \sin(2\phi)|^2 \\
 &= [1 - r_1 r_2 \cos(2\phi)]^2 + r_1^2 r_2^2 \sin^2(2\phi) \\
 &= 1 + R_1 R_2 - 2\sqrt{R_1 R_2} \cos(2\phi) = (1 - \sqrt{R_1 R_2})^2 + 4\sqrt{R_1 R_2} \sin^2(\phi),
 \end{aligned} \tag{15.16}$$

$$\begin{aligned}
 |r_1 - r_2 e^{-i2\phi}|^2 &= |r_1 - r_2 \cos(2\phi) + i r_2 \sin(2\phi)|^2 \\
 &= [r_1 - r_2 \cos(2\phi)]^2 + [r_2 \sin(2\phi)]^2 \\
 &= R_1 + R_2 - 2\sqrt{R_1 R_2} \cos(2\phi) \\
 &= R_1 + R_2 - 2\sqrt{R_1 R_2} [1 - 2\sin^2(\phi)] \\
 &= (\sqrt{R_1} - \sqrt{R_2})^2 + 4\sqrt{R_1 R_2} \sin^2(\phi).
 \end{aligned} \tag{15.17}$$

The generic Airy distribution, which considers solely the physical processes exhibited by light inside the resonator, then derives as the intensity circulating in the resonator relative to the intensity launched, which by use of Eqs. (15.15) and (15.16) yields

$$\begin{aligned}
 A_{circ} &= \frac{I_{circ}}{I_{laun}} = \frac{|E_{circ}|^2}{|E_{laun}|^2} = \frac{1}{|1 - r_1 r_2 e^{-i2\phi}|^2} \\
 &= \frac{1}{(1 - \sqrt{R_1 R_2})^2 + 4\sqrt{R_1 R_2} \sin^2(\phi)}.
 \end{aligned} \tag{15.18}$$

Physically, A_{circ} represents the spectrally dependent internal resonance enhancement which the resonator provides to the light launched into it. It is displayed for different mirror reflectivities in Fig. 15.2. At the resonance frequencies ν_q , where $\sin(\phi)$ equals zero, the internal resonance enhancement factor is

$$A_{circ}(\nu_q) = \frac{1}{(1 - \sqrt{R_1 R_2})^2}. \tag{15.19}$$

15.3.2 Other Airy Distributions

Once generic Airy distribution of Eq. (15.18), is established, all other Airy distributions, i.e., the observed light intensities relative to the launched or initial intensity from the light source (Fig. 15.1) can then be straight-forwardly deduced by simple scaling factors. Since the intensity launched into the resonator equals the transmitted fraction of the intensity incident upon mirror 1,

$$I_{laun} = (1 - R_1) I_{inc}, \tag{15.20}$$

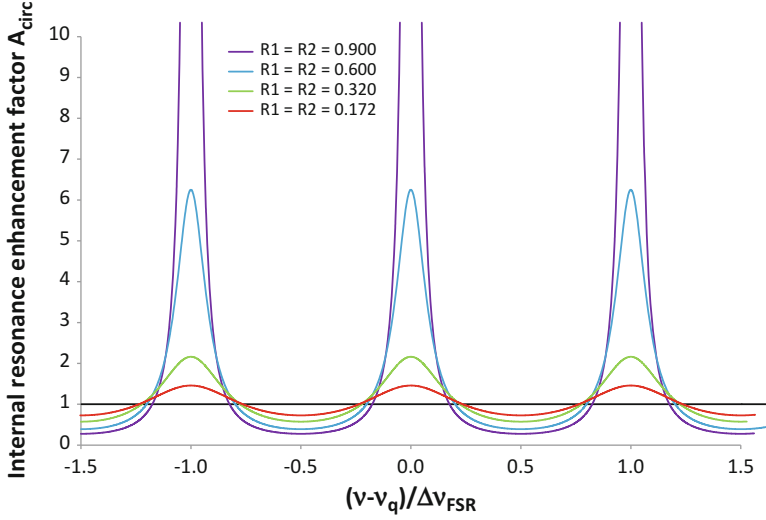


Fig. 15.2 Generic Airy distribution A_{circ} , equaling the spectrally dependent internal resonance enhancement which the resonator provides to light that is launched into it. For the curve with $R_1 = R_2 = 0.9$, the peak value is at $A_{circ}(v_q) = 100$, outside the scale of the ordinate. (Figure taken from Ref. [10])

and the intensities transmitted through mirror 2, reflected at mirror 2, and transmitted through mirror 1 are the transmitted and reflected/transmitted fractions of the intensity circulating inside the resonator,

$$I_{trans} = (1 - R_2) I_{circ}, I_{b-circ} = R_2 I_{circ}, I_{back} = (1 - R_1) I_{b-circ} \quad (15.21)$$

respectively, one obtains the following Airy distributions:

$$A_{b-circ} = \frac{I_{b-circ}}{I_{laun}} = R_2 A_{circ}, \quad (15.22)$$

$$A_{trans} = \frac{I_{trans}}{I_{laun}} = (1 - R_2) A_{circ}, \quad (15.23)$$

$$A_{back} = \frac{I_{back}}{I_{laun}} = (1 - R_1) R_2 A_{circ}, \quad (15.24)$$

$$A_{emit} = A_{trans} + A_{back} = \frac{I_{trans} + I_{back}}{I_{laun}} = (1 - R_1 R_2) A_{circ}, \quad (15.25)$$

$$A'_{circ} = \frac{I_{circ}}{I_{inc}} = (1 - R_1) A_{circ}, \quad (15.26)$$

$$A'_{b-circ} = \frac{I_{b-circ}}{I_{inc}} = (1 - R_1) R_2 A_{circ}, \quad (15.27)$$

$$A'_{trans} = \frac{I_{trans}}{I_{inc}} = (1 - R_1) (1 - R_2) A_{circ}, \quad (15.28)$$

$$A'_{back} = \frac{I_{back}}{I_{inc}} = (1 - R_1)^2 R_2 A_{circ}, \quad (15.29)$$

$$\begin{aligned} A'_{emit} &= A'_{trans} + A'_{back} = \frac{I_{trans} + I_{back}}{I_{inc}} \\ &= (1 - R_1) (1 - R_1 R_2) A_{circ}. \end{aligned} \quad (15.30)$$

The index “emit” denotes Airy distributions that consider the sum of intensities emitted on both sides of the resonator. The prime denotes Airy distributions with respect to the incident intensity I_{inc} .

The back-transmitted intensity I_{back} cannot be measured, because also the initially back-reflected light adds to the backward-propagating signal. The measurable case of the intensity resulting from the interference of both backward-propagating electric fields is derived as follows. The back-transmitted electric field is

$$E_{back} = it_1 r_2 E_{circ} e^{-i2\phi} \Rightarrow \frac{E_{back}}{E_{inc}} = \frac{-t_1^2 r_2 e^{-i2\phi}}{1 - r_1 r_2 e^{-i2\phi}}. \quad (15.31)$$

Including the initially back-reflected electric field, $E_{refl,1} = r_1 E_{inc}$, the total electric field propagating backward from mirror 1 is

$$\frac{E_{refl}}{E_{inc}} = \frac{E_{refl,1} + E_{back}}{E_{inc}} = r_1 + \frac{-t_1^2 r_2 e^{-i2\phi}}{1 - r_1 r_2 e^{-i2\phi}} = \frac{r_1 - r_2 e^{-i2\phi}}{1 - r_1 r_2 e^{-i2\phi}}. \quad (15.32)$$

Exploiting Eqs. (15.15, 15.16, and 15.17), the total relative intensity propagating backward from mirror 1 amounts to

$$\begin{aligned} A'_{refl} &= \frac{I_{refl}}{I_{inc}} = \frac{|E_{refl}|^2}{|E_{inc}|^2} = \frac{|r_1 - r_2 e^{-i2\phi}|^2}{|1 - r_1 r_2 e^{-i2\phi}|^2} = \frac{(\sqrt{R_1} - \sqrt{R_2})^2 + 4\sqrt{R_1 R_2} \sin^2(\phi)}{(1 - \sqrt{R_1 R_2})^2 + 4\sqrt{R_1 R_2} \sin^2(\phi)} \\ &\Rightarrow A'_{trans} + A'_{refl} = \frac{I_{trans} + I_{refl}}{I_{inc}} = 1, \end{aligned} \quad (15.33)$$

as expected for a resonator that exhibits only outcoupling losses. At the resonance frequencies, the back-emitted electric field E_{back} destructively interferes with the electric field $E_{refl,1}$ initially back-reflected.

A'_{circ} of Eq. (15.26) represents the external resonance enhancement factor with respect to I_{inc} . The external resonance enhancement factor at the resonance frequencies is

$$A'_{circ}(\nu_q) = \frac{(1 - R_1)}{(1 - \sqrt{R_1 R_2})^2} = (1 - R_1) A_{circ}(\nu_q). \tag{15.34}$$

In experimental situations, often light is transmitted through a Fabry-Pérot resonator in order to characterize the resonator or to use it as a scanning interferometer (see later in Sect. 15.4). Therefore, an often applied Airy distribution is A'_{trans} of Eq. (15.28). It describes the fraction I_{trans} of the intensity I_{inc} of a light source incident upon mirror 1 that is transmitted through mirror 2, see Fig. 15.1. A'_{trans} is displayed in Fig. 15.3 (solid lines) for different values of the reflectivities $R_1 = R_2$. Its peak value at the resonance frequencies ν_q is

$$A'_{trans}(\nu_q) = \frac{(1 - R_1)(1 - R_2)}{(1 - \sqrt{R_1 R_2})^2} \stackrel{R_1=R_2}{=} 1. \tag{15.35}$$

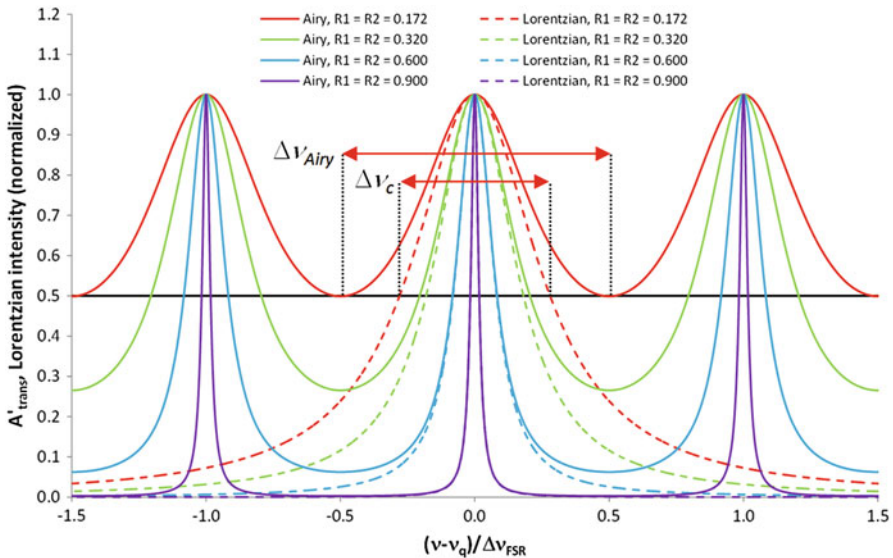


Fig. 15.3 Airy distribution A'_{trans} (solid lines), corresponding to light transmitted through a Fabry-Pérot resonator, calculated from Eq. (15.28) for different values of the reflectivities $R_1 = R_2$, and comparison with a single Lorentzian line (dashed lines) calculated from Eq. (15.13) for the same $R_1 = R_2$. At half maximum (black line), with decreasing reflectivities the FWHM linewidth $\Delta\nu_{Airy}$ of the Airy distribution broadens compared to the FWHM linewidth $\Delta\nu_c$ of its corresponding Lorentzian line: $R_1 = R_2 = 0.9, 0.6, 0.32, 0.172$ results in $\Delta\nu_{Airy}/\Delta\nu_c = 1.001, 1.022, 1.132, 1.717$, respectively. (Figure taken from Ref. [10])

15.3.3 Airy Distribution As a Sum of Mode Profiles

In Fig. 15.3 one observes that, at high reflectivity, there is almost perfect agreement between the spectral shape of the Airy distribution (solid purple line) and its underlying Lorentzian lines (dashed purple line), i.e., the former is rather well represented by the latter. This fact has prompted Saleh and Teich [6] to propose that in this case the Airy linewidth $\Delta\nu_{Airy}$ of a Fabry-Pérot resonator is similar to the linewidth $\Delta\nu_c = 1/(2\pi\tau_c)$ of its underlying Lorentzian lines, both defined as FWHM (black line). However, as is generally well known, with decreasing reflectivity the linewidth of the Airy distribution (solid lines) broadens faster than that of the underlying Lorentzian lines (dashed lines).

Svelto [5] attributes this discrepancy to Eq. (15.5) being only an approximation, thereby implicating that also Eq. (15.11) is only an approximation, such that the Airy linewidth $\Delta\nu_{Airy}$ of a Fabry-Pérot resonator can only at high reflectivity be approximated by the linewidth $\Delta\nu_c$ of its underlying Lorentzian lines. We will demonstrate that the discrepancy has a different reason.

According to Koppelman [11], Bayer-Helms [12] “showed that the Airy distribution can be represented exactly” by the sum of Lorentzian spectral line shapes times a calibration factor. Firstly, while being literally correct, this statement is physically misleading, secondly, the calibration factor used in [11] remains unexplained, thirdly, the equivalence is shown only for equal reflectivities, $R_1 = R_2$, and finally, the equivalence is not investigated for non-Lorentzian spectral line shapes.

Here we verify that the Airy distribution is nothing else but the sum of the mode profiles of the longitudinal resonator modes, thereby revealing the physical origin of the Airy distribution. Our approach starts from the electric field E_{circ} circulating inside the resonator, considers the exponential decay in time of this field through both mirrors of the resonator, see Fig. 15.1, Fourier transforms it to frequency space according to Eq. (15.10) to obtain the normalized spectral line shapes $\tilde{\gamma}_q(\nu)$ of Eq. (15.11), divides it by the round-trip time t_{RT} to account for how the total circulating electric-field intensity is longitudinally distributed in the resonator and coupled out per unit time, resulting in the emitted mode profiles,

$$\gamma_{q,emit}(\nu) = \frac{1}{t_{RT}} \tilde{\gamma}_q(\nu), \quad (15.36)$$

in units of (1), and then sums over the emitted mode profiles of all longitudinal modes at positive, zero, and negative frequencies. Consequently, the sum of emitted mode profiles describes an experiment that must result in the Airy distribution A_{emit} of Eq. (15.25). Exploiting the derivation given in Appendix C of [10], the sum of emitted mode profiles of Eq. (15.36) yields

$$\sum_{q=-\infty}^{\infty} \gamma_{q,emit}(\nu) = \frac{1 - R_1 R_2}{(1 - \sqrt{R_1 R_2})^2 + 4\sqrt{R_1 R_2} \sin^2(\phi)} = A_{emit}, \quad (15.37)$$

which is indeed equal to Eq. (15.25), with Eq. (15.18) inserted. Each spectral line shape $\tilde{\gamma}_q(\nu)$ of Eq. (15.11) and mode profile $\gamma_{q, emit}(\nu)$ of Eq. (15.36) is extended over the infinite frequency range, consequently light at a specific frequency ν inside the resonator excites all longitudinal modes of the resonator. However, the contributions from different longitudinal modes to the light at frequency ν do not interfere with each other, because all optical modes are orthogonal with each other. For this reason, the sum in Eq. (15.37) is over the intensity mode profiles $\gamma_{q, emit}(\nu)$ rather than over the electric fields. Because of resonant enhancement of the launched light the peak value of A_{emit} at the resonance frequencies ν_q ,

$$A_{emit}(\nu_q) = \frac{1 - R_1 R_2}{(1 - \sqrt{R_1 R_2})^2} = \frac{1 + \sqrt{R_1 R_2}}{1 - \sqrt{R_1 R_2}} > 1, \quad (15.38)$$

becomes larger than unity. Nevertheless, because of Eqs. (15.20) and (15.33) the energy of the system is conserved.

The observation that with decreasing R_1 and R_2 the linewidth of the resulting Airy distribution in Fig. 15.3 is increasingly broader than the linewidth of the underlying Lorentzian lines simply arises from the fact that one sums up mode profiles (with the same linewidth as the Lorentzian lines) that resonate at different frequencies. It does not constitute a discrepancy, as has often been proposed.

The derivation shown here demonstrates that—from a physical point of view—the spectral line shapes and mode profiles are the fundamental spectral functions that characterize the Fabry-Pérot resonator and their sum quantifies its spectral response. As we will see in Sect. 15.4, this fundamental understanding has direct consequences for the definitions of linewidth and finesse.

The same simple scaling factors of Eqs. (15.20) and (15.21) that provide the relations between the individual Airy distributions, see Eqs. (15.18) and (15.22, 15.23, 15.24, 15.25, 15.26, 15.27, 15.28, 15.29, 15.30), also provide the relations among $\gamma_{q, emit}(\nu)$ and the other mode profiles:

$$\begin{aligned} \gamma_{q, circ} &= \frac{1}{R_2} \gamma_{q, b-circ} = \frac{1}{1-R_2} \gamma_{q, trans} = \frac{1}{1-R_1} \gamma_{q, back} = \frac{1}{1-R_1 R_2} \gamma_{q, emit} \\ \gamma'_{q, circ} &= \frac{1}{R_2} \gamma'_{q, b-circ} = \frac{1}{1-R_2} \gamma'_{q, trans} = \frac{1}{1-R_1} \gamma'_{q, back} = \frac{1}{1-R_1 R_2} \gamma'_{q, emit} \\ &= (1 - R_1) \gamma_{q, circ}. \end{aligned} \quad (15.39)$$

The various mode profiles $\gamma_q(\nu)$ and $\gamma'_q(\nu)$ are calibrated with respect to the launched and the incident intensity, respectively, and the sum over one of these mode profiles at all resonance frequencies generates the corresponding Airy distribution.

15.4 Lorentzian Linewidth and Finesse Versus Airy Linewidth and Finesse

A commonly accepted definition of spectral resolution the Taylor criterion [13]. It proposes that two spectral lines can be resolved if the individual lines cross at half intensity. In the case of two identical, symmetric spectral lines their peaks would then be separated by their FWHM. The Taylor criterion is utilized in the following.

15.4.1 Characterizing the Fabry–Pérot Resonator: Lorentzian Linewidth and Finesse

When launching light into the Fabry–Pérot resonator in a non-scanning experiment, i.e., at fixed resonator length (and fixed angle of incidence), the Fabry–Pérot resonator becomes the object of investigation. The spectral line shapes, Lorentzian lines, and mode profiles are the fundamental functions. By measuring the sum of mode profiles, the Airy distribution, one can derive the total loss of the Fabry–Pérot resonator via recalculating the Lorentzian linewidth $\Delta\nu_c$ of Eq. (15.12), displayed (blue line) relative to the free spectral range in Fig. 15.4a, c.

The underlying Lorentzian lines can be resolved as long as the Taylor criterion is obeyed (Fig. 15.5). Consequently, one can define a parameter which we call the Lorentzian finesse of a Fabry–Pérot resonator:

$$F_c := \frac{\Delta\nu_{FSR}}{\Delta\nu_c} = \frac{2\pi}{-\ln(R_1 R_2)}. \quad (15.40)$$

It is displayed as the blue line in Fig. 15.4b, d. The Lorentzian finesse F_c has a fundamental physical meaning: it describes how well the Lorentzian lines underlying the Airy distribution can be resolved when measuring the Airy distribution. A Fabry–Pérot resonator generating single-longitudinal-mode laser light is characterized by its Lorentzian linewidth and finesse.

Since $\Delta\nu_c$ exists for any mirror reflectivity, the definition of the Lorentzian finesse does not break down at a critical value. However, at the point where

$$\Delta\nu_c = \Delta\nu_{FSR} \Rightarrow R_1 R_2 = e^{-2\pi} \approx 0.001867, \quad (15.41)$$

equivalent to $F_c = 1$, the Taylor criterion for the spectral resolution of a single Airy distribution is reached. For equal mirror reflectivities, this point occurs when $R_1 = R_2 \approx 4.32\%$. Therefore, the linewidth of the Lorentzian lines underlying the Airy distribution of a Fabry–Pérot resonator can be resolved by measuring the Airy distribution, hence its resonator losses can be spectroscopically determined, until this point. Obviously, the Lorentzian finesse according to the definition of

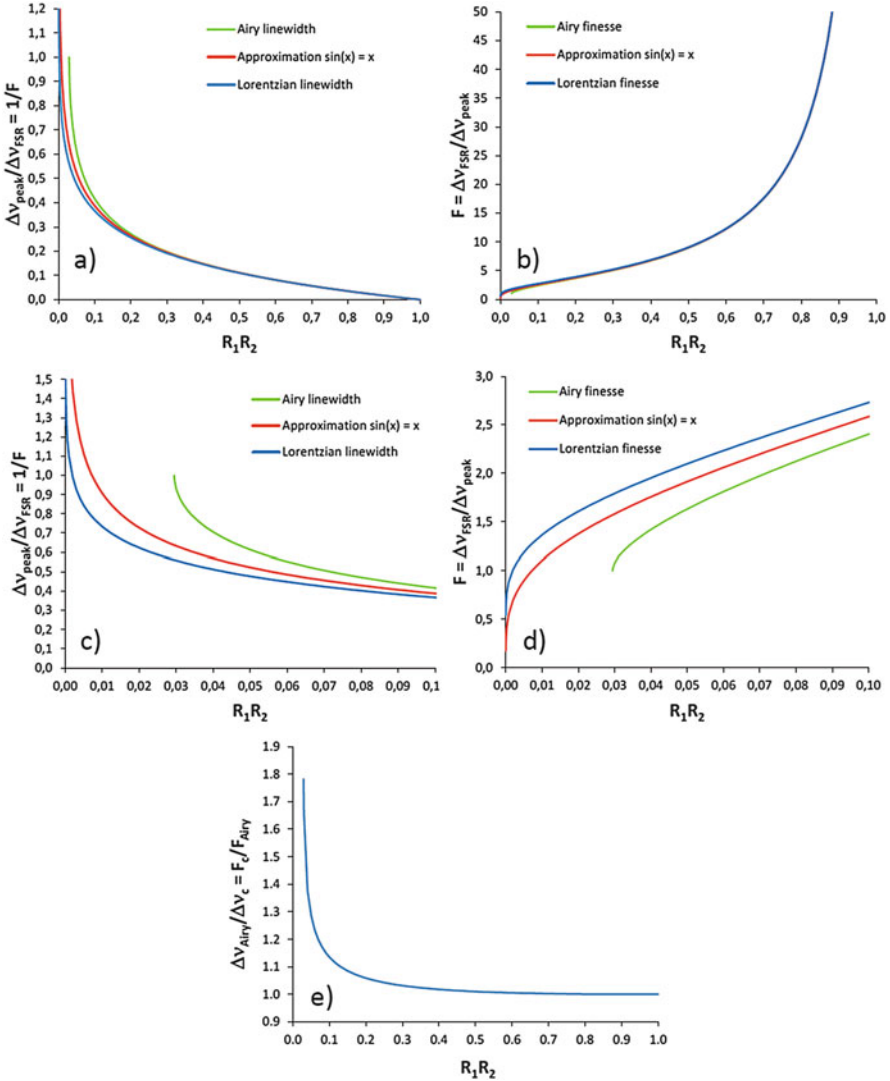


Fig. 15.4 (a) Relative Lorentzian linewidth $\Delta v_c / \Delta v_{FSR}$, with Δv_c from Eq. (15.12) (blue curve), relative Airy linewidth $\Delta v_{Airy} / \Delta v_{FSR}$, with Δv_{Airy} from Eq. (15.43) (green curve), and its approximation of Eq. (15.46) (red curve), and (b) Lorentzian finesse F_c of Eq. (15.40) (blue curve), Airy finesse F_{Airy} of Eq. (15.45) (green curve), and its approximation of Eq. (15.47) (red curve) as a function of reflectivity value $R_1 R_2$. (c and d) Zoom into the low-reflectivity region. The exact solutions of the Airy linewidth and finesse (green lines) correctly break down at $\Delta v_{Airy} = \Delta v_{FSR}$, equivalent to $F_{Airy} = 1$, whereas their approximations (red lines) do not break down. (e) Ratio between the Airy linewidth Δv_{Airy} of Eq. (15.43) and the Lorentzian linewidth Δv_c of Eq. (15.12), equaling the ratio between the Lorentzian finesse F_c of Eq. (15.40) and the Airy finesse F_{Airy} of Eq. (15.45), as a function of reflectivity value $R_1 R_2$. (Figure taken from Ref. [10])

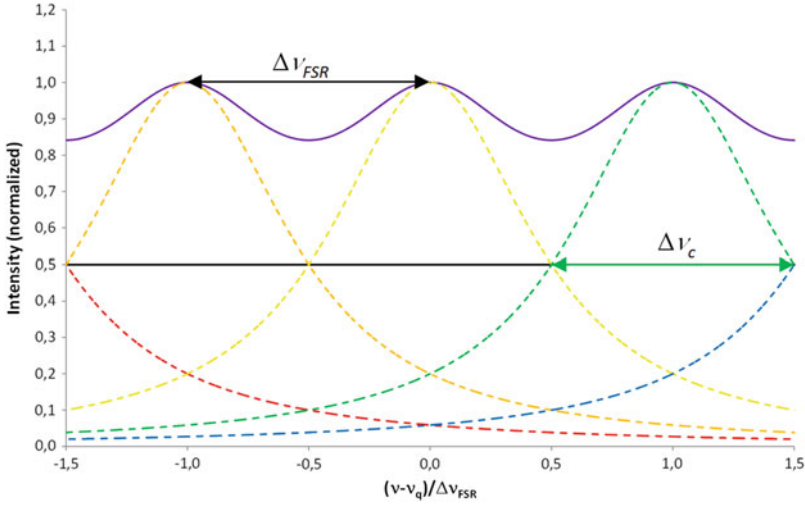


Fig. 15.5 Illustration of the physical meaning of the Lorentzian finesse F_c of a Fabry-Pérot resonator. Displayed is the situation for $R_1 = R_2 \approx 4.32\%$, at which $\Delta v_c = \Delta v_{FSR}$ and $F_c = 1$, i.e., two adjacent Lorentzian lines (dashed colored lines, only 5 lines are shown for clarity) cross at half maximum (solid black line) and the Taylor criterion for spectrally resolving two peaks in the resulting Airy distribution (solid purple line) is reached. (Figure taken from Ref. [10])

Eq. (15.40) plays an essential role in the characterization of low-reflectivity or otherwise high-loss Fabry-Pérot resonators.

15.4.2 Scanning the Fabry-Pérot Resonator: Airy Linewidth and Finesse

A different situation occurs when the Fabry-Pérot resonator is used as a scanning interferometer, i.e., at varying resonator length (or angle of incidence), to spectroscopically distinguish spectral lines at different frequencies within one free spectral range. In this case several Airy distributions, each one created by an individual spectral line, must be resolved. Therefore, now the Airy distribution becomes the underlying fundamental function and the measurement delivers a sum of Airy distributions. The parameters that properly quantify this situation are the Airy linewidth Δv_{Airy} and the Airy finesse F_{Airy} .

On either side of the peak of Eq. (15.35) located at ν_q , the transmitted intensity decreases to $A'_{trans}(\nu_q)/2$ when the phase shift ϕ changes by the amount $\Delta\phi$ and, accordingly, $\sin^2(\phi)$ changes from 0, such that in the denominator of A_{circ} of Eq. (15.18)

$$4\sqrt{R_1 R_2} \sin^2(\Delta\phi) = \left(1 - \sqrt{R_1 R_2}\right)^2 \Rightarrow \Delta\phi = \arcsin\left(\frac{1 - \sqrt{R_1 R_2}}{2\sqrt[4]{R_1 R_2}}\right). \quad (15.42)$$

Exploiting Eqs. (15.6) and (15.7) to calculate $\phi = \pi\nu/\Delta\nu_{FSR}$, resulting in $\Delta\phi = \pi(\Delta\nu_{Airy}/2)/\Delta\nu_{FSR}$, then provides the FWHM linewidth $\Delta\nu_{Airy}$ of the Airy distribution [3],

$$\Delta\nu_{Airy} = \Delta\nu_{FSR} \frac{2}{\pi} \arcsin\left(\frac{1 - \sqrt{R_1 R_2}}{2\sqrt[4]{R_1 R_2}}\right). \quad (15.43)$$

The Airy linewidth $\Delta\nu_{Airy}$ is displayed as the green curve in Fig. 15.4a, c in direct comparison with the Lorentzian linewidth $\Delta\nu_c$. The ratio between $\Delta\nu_{Airy}$ of Eq. (15.43) and $\Delta\nu_c$ of Eq. (15.12) is displayed in Fig. 15.4e.

The concept of defining the linewidth of the Airy peaks as FWHM breaks down at $\Delta\nu_{Airy} = \Delta\nu_{FSR}$ (solid red line in Fig. 15.3), because at this point the Airy linewidth instantaneously jumps to an infinite value. For lower reflectivity values $R_1 R_2$, the FWHM linewidth of the Airy peaks is undefined and other definitions or concepts would have to be utilized to describe the situation. The limiting case occurs at

$$\Delta\nu_{Airy} = \Delta\nu_{FSR} \Rightarrow \frac{1 - \sqrt{R_1 R_2}}{2\sqrt[4]{R_1 R_2}} = 1 \Rightarrow R_1 R_2 = 17 - 12\sqrt{2} \approx 0.02944. \quad (15.44)$$

For equal mirror reflectivities, this point is reached when $R_1 = R_2 \approx 17.2\%$ (solid red line in Fig. 15.3).

The finesse of the Airy distribution of a Fabry-Pérot resonator, which is displayed as the green curve in Fig. 15.4b, d in direct comparison with the Lorentzian finesse F_c , is properly defined as

$$F_{Airy} \stackrel{!}{:=} \frac{\Delta\nu_{FSR}}{\Delta\nu_{Airy}} = \frac{\pi}{2} \left[\arcsin\left(\frac{1 - \sqrt{R_1 R_2}}{2\sqrt[4]{R_1 R_2}}\right) \right]^{-1}. \quad (15.45)$$

When scanning the length of the Fabry-Pérot resonator (or alternatively the angle of incident light), the Airy finesse lucidly quantifies the maximum number of Airy distributions created by light at individual frequencies ν_m within the free spectral range of the Fabry-Pérot resonator, whose adjacent peaks can be unambiguously distinguished spectroscopically, i.e., they do not overlap at their FWHM (Fig. 15.6). Consequently, this definition of the Airy finesse is consistent with the Taylor criterion of the resolution of a spectrometer and is, therefore, denoted by an exclamation mark in Eq. (15.45). Since the concept of the FWHM linewidth breaks

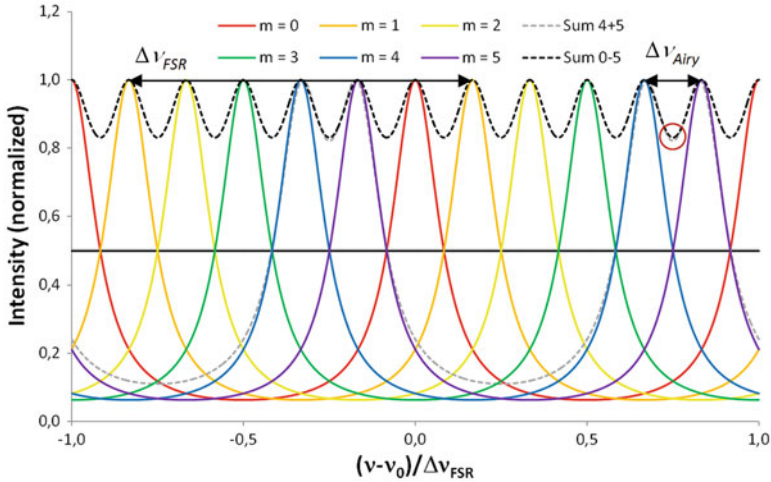


Fig. 15.6 Illustration of the physical meaning of the Airy finesse F_{Airy} of a Fabry-Pérot resonator. When scanning the Fabry-Pérot length (or alternatively the angle of incident light), Airy distributions (solid lines) are created by signals at individual frequencies. If the signals occur at frequencies $\nu_m = \nu_q + m\Delta\nu_{Airy}$, where m is an integer starting at q , the Airy distributions at adjacent frequencies are separated from each other by the linewidth $\Delta\nu_{Airy}$, thereby fulfilling the Taylor criterion for the spectroscopic resolution of two adjacent peaks. The maximum number of signals that can be resolved is F_{Airy} . Since in this specific example the reflectivities $R_1 = R_2 = 0.59928$ have been chosen such that $F_{Airy} = 6$ is an integer, the signal for $m = F_{Airy}$ at the frequency $\nu_q + F_{Airy}\Delta\nu_{Airy} = \nu_q + \Delta\nu_{FSR}$ coincides with the signal for $m = q$ at ν_q . In this example, a maximum of $F_{Airy} = 6$ peaks can be resolved when applying the Taylor criterion. However, the sum of two adjacent “resolvable” peaks (dashed gray line) exhibits a deeper dip between the adjacent peaks to be resolved, i.e., a better resolution, than the sum of all “resolvable” peaks (dashed black line), see the difference highlighted in the red circle. (Figure taken from Ref. [10])

down at $\Delta\nu_{Airy} = \Delta\nu_{FSR}$, consequently the Airy finesse is defined only until $F_{Airy} = 1$, see Fig. 15.4d, because the arcsin function in Eq. (15.45) cannot produce values above $\pi/2$.

Generally, one can argue that the Taylor criterion leaves some ambiguity to the definition of the limit of spectral resolution, because it does not state whether it requires the absence or allows for the presence of additional resolvable spectral lines. In the example of Fig. 15.6, the sum of two adjacent “resolvable” Airy distributions (dashed gray line) is better resolvable than the sum of all “resolvable” Airy distributions (dashed black line), because in the latter case additional Airy distributions contribute, see the dashed lines within the red circle in Fig. 15.6. If either of the two options defines the limit of spectral resolution, the other cannot.

15.4.3 Questionable Approximations and Definitions

Often the unnecessary approximation $\sin(\phi) \approx \phi$ is made when deriving from A'_{trans} of Eq. (15.28) the Airy linewidth [2, 4]. In contrast to the exact Eqs. (15.42) and (15.43), it leads to

$$4\sqrt{R_1 R_2}(\Delta\phi)^2 \approx (1 - \sqrt{R_1 R_2})^2 \Rightarrow \Delta\nu_{Airy} \approx \Delta\nu_{FSR} \frac{2}{\pi} \Delta\phi = \Delta\nu_{FSR} \frac{1}{\pi} \frac{1 - \sqrt{R_1 R_2}}{\sqrt{R_1 R_2}}. \quad (15.46)$$

This approximation of the Airy linewidth, displayed as the red curve in Fig. 15.4a, c, deviates from the correct curve at low reflectivities and incorrectly does not break down when $\Delta\nu_{Airy} > \Delta\nu_{FSR}$. This approximation is then typically also inserted into Eq. (15.45) to calculate the Airy finesse [4], resulting in

$$F_{Airy} \stackrel{!}{:=} \frac{\Delta\nu_{FSR}}{\Delta\nu_{Airy}} \approx \pi \frac{\sqrt[4]{R_1 R_2}}{1 - \sqrt{R_1 R_2}}. \quad (15.47)$$

Vaughan [2] and Siegman [3] even defined the Airy finesse by its approximation of Eq. (15.47),

$$\widehat{F}_{Airy} \stackrel{?}{:=} \pi \frac{\sqrt[4]{R_1 R_2}}{1 - \sqrt{R_1 R_2}} \approx \frac{\Delta\nu_{FSR}}{\Delta\nu_{Airy}}, \quad (15.48)$$

thereby depriving this parameter of its lucid meaning. Since the definition of Eq. (15.48) does not comply with the Taylor criterion, it is denoted by a question mark. Saleh and Teich [7, 8] also proposed Eq. (15.48) for the Airy finesse, but from their derivation it remains unclear whether they consider it as a definition or as an approximation of Eq. (15.45).

15.4.4 Response to Frequency-Dependent Reflectivity

In the previous Sections we described a Fabry-Pérot resonator whose mirror reflectivities are independent of frequency. We showed that the Airy distribution is nothing else but the sum of its underlying mode profiles. Now we consider the mirror reflectivities as general functions of frequency, $R_i(\nu)$, such that the photon-decay time $\tau_c(\nu)$ of Eq. (15.3) becomes a function of frequency. As a result, the spectral line shapes $\tilde{\gamma}_q(\nu)$ of Eq. (15.11), the mode profiles $\gamma_{q, emit}(\nu)$ of Eq. (15.36) and all other mode profiles, as well as the Airy distribution $A_{emit}(\nu)$ of Eq. (15.37) and all other Airy distributions, are spectrally modified. In Eqs. (15.12) and (15.13), $\Delta\nu_c$ turns into a local function of frequency, thereby losing its meaning as the FWHM linewidth. Nevertheless, all Airy distributions fundamentally remain the sums of their corresponding mode profiles. Consequently, even for frequency-dependent

reflectivities $R_i(\nu)$ we can calculate the spectral line shape $\tilde{\gamma}_q(\nu)$ and mode profile $\gamma_{q, emit}(\nu)$ of each mode directly from Eqs. (15.11) and (15.36), respectively, and obtain all other mode profiles via the simple scaling factors of Eq. (15.39).

15.5 Summary

The understanding that the Airy distribution describing the spectral transmission of a Fabry-Pérot resonator physically originates in the sum of mode profiles of the longitudinal resonator modes has fundamental consequences. The resonator losses are related to the linewidth of the Lorentzian lines rather than the linewidth of the Airy distribution. Hence, a new parameter, the Lorentzian finesse, becomes important. Once the internal resonance enhancement, equaling the generic Airy distribution that characterizes the light intensity that is forward circulating inside the resonator, is known, all other Airy distributions of back-circulating, transmitted, back-transmitted, and total emitted light intensity can be derived by simple scaling factors. Furthermore, in the case of frequency-dependent mirror reflectivities, the deformed spectral line shapes and mode profiles of the underlying modes can be derived from the same simple equations. Also in this generalized situation, each sum of mode profiles generates the corresponding Airy distribution.

Acknowledgments The authors thank Cristine C. Kores and Dimitri Geskus for their contributions and acknowledge financial support by the ERC Advanced Grant “Optical Ultra-Sensor” No. 341206 from the European Research Council.

References

1. Fabry C, Pérot A (1899) Theorie et applications d’une nouvelle methode de spectroscopie interferentielle. *Ann de Chim et de Phys* 16:115
2. Vaughan JM (1989) The Fabry-Pérot interferometer. Adam Hilger, Bristol/Philadelphia, ch. 3
3. Siegman AE (1986) Lasers. University Science Books, Mill Valley, ch. 11
4. Svelto O (2010) Principles of lasers, 5th edn. Springer, New York, pp 142–146, ch. 4.5.1
5. Svelto O (2010) Principles of lasers, 5th edn. Springer, New York, pp 169–171, ch. 5.3
6. Saleh BEA, Teich MC (2007) Fundamentals of photonics, 2nd edn. Wiley-Interscience, Hoboken, pp 571–572
7. Saleh BEA, Teich MC (2007) Fundamentals of photonics, 2nd edn. Wiley-Interscience, Hoboken, pp 254–257, ch. 7.1B
8. Saleh BEA, Teich MC (2007) Fundamentals of photonics, 2nd edn. Wiley-Interscience, Hoboken, pp 62–66, ch. 2.5B
9. Eichhorn M, Pollnau M (2015) Spectroscopic foundations of lasers: spontaneous emission into a resonator mode. *IEEE J Sel Top Quantum Electron* 21:9000216
10. Ismail N, Kores CC, Geskus D, Pollnau M (2016) Fabry-Perot resonator: spectral line shapes, generic and related Airy distributions, linewidths, finesses, and performance at low or frequency-dependent reflectivity. *Opt Express* 24:16366

11. Koppelmann G (1969) Multiple-beam interference and natural modes in open resonators. In: Wolf E (ed) *Progress in optics*, vol 7. North Holland, Amsterdam/London, pp 1–66, ch. 1
12. Bayer-Helms F (1963) Analyse von Linienprofilen. I Grundlagen und Messeinrichtungen. *Z Phys* 15:330
13. Juvells I, Carnicer A, Ferré-Borrull J, Martín-Badosa E, Montes-Usategui M (2006) Understanding the concept of resolving power in the Fabry-Perot interferometer using a digital simulation. *Eur J Phys* 27:1111